SOME ASPECTS OF GOLD–GOLD COLLISIONS AT RHIC AT $\sqrt{s_{NN}} = 200$ GeV AND A VERSION OF THE SEQUENTIAL CHAIN MODEL

P. GUPTAROY

Department of Physics, Raghunathpur College,
P.O. Raghunathpur 723133 Dist., Purulia (WB), India
gpradeepta@rediffmail.com

BHASKAR DE

Department of Physics, Moulana Azad College, Kolkata-700013, India

GOUTAM SAU

Beramara Ram Chandrapur High School, South 24-Pgs, 743609 (WB), India
gautamsau@yahoo.co.in

S. K. BISWAS

West Kodalia Adarsha Siksha Sadan, New Barrackpore, Kolkata-700131, India
sunil_biswas2004@yahoo.com

S. BHATTACHARYYA*

Physics and Applied Mathematics Unit (PAMU),
Indian Statistical Institute, Kolkata-700108, India
bsubrata@isical.ac.in

Received 24 February 2007
Revised 17 May 2007

Experimental studies on gold–gold collisions at RHIC at $\sqrt{s_{NN}} = 200$ GeV have produced a vast amount of data and results to be analyzed in the light of various competing models in the domain of multiparticle production scenario. We have chosen to analyze here the measured data on the p_T-spectra of various light and nonstrange secondaries and some of their very important ratio-behaviors at the various centralities of the collision in the light of a version of the sequential chain model. The agreements between measured data and theoretical plots are found to be modestly satisfactory.

Keywords: Relativistic heavy ion collisions; inclusive production; quark–gluon plasma.

PACS numbers: 25.75.-q, 13.85.Ni, 12.38.Mh

*Corresponding author.

1. Introduction

Multiple production of secondaries in heavy ion collisions is a topic of very current interest.[1–14] There are several reasons for it. First, this field provides some insights into the parton structure of the nucleus[1–7] and the nature of high energy nuclear collisions.[13,14] Second, this topic offers a very crucial testing ground for verifying the quantum chromodynamical predictions about the formation of quark–gluon plasma (QGP) at high density and pressure.[13,14] Third, the particle and high energy nuclear physicists, by and large, believe that the relevant studies would lead to the formation of a decisive verdict on the QCD-based phase transition ideas.[15–18,a] Fourth, as the nucleus–nucleus interactions at high energies involve large number of participants and their multiple collisions, there is a strong likelihood that the probable collective effects which supposedly influence the production of the secondaries could arise. It is believed that the studies would throw light on the existence of these collective effects.

After nearly five-year experimental searches for detecting the QGP state at RHIC, the final outcome, so far, is the consensus on the existence of only a new (but undefined?) state of matter but not any trace of what was earlier hypothesized to be the QGP-state.[8–11,19–22] So, in our approach, we have diverted our attention from both the QCD- and QGP-based viewpoints and, instead, we have introduced some alternative ideas and a version of the sequential chain model (SCM) for understanding the available data on the relatively more abundant variety of hadrons, i.e. pions, kaons, and protons–antiprotons. We would like to deal, in this work, with the production of these most important varieties of secondaries, and also with some relevant ratio behaviors which would help cross-check the used working formulas on the p_T-spectra.

The paper would be organized as follows. In Sec. 2 we have presented the broad outline of the theoretical underpinnings of this work with induction of some new and nontypical ideas. In Sec. 3 the model confronts the measured data; and the results obtained by our approaches are represented by numerous figures and tables *vis-a-vis* the experimental data. The last section (Sec. 4) summarizes the conclusions and final comments.

2. The Theoretical Framework: Approaches to High Energy NN and AA Collisions

Here, in the first subsection, we deal with the production of the pions, kaons and proton–antiprotons in nucleon–nucleon (NN) interactions. Subsequently, in the next one, we concentrate on the approach for converting the results of NN collision to the corresponding value for the case nucleus–nucleus (AA) collision.

[a] http://info.web.cern.ch/Press/PressReleases/Releases2000/PRO1.00EQuarkGluonMatter.html.

2.1. *Nucleon–nucleon collisions at high energies and a specific multiple production model*

At the very start, we describe and state some of the salient features and important physical characteristics of the SCM valid for hadron–hadron collisions.[23–34] According to this model, high energy hadronic interactions boil down, essentially, to the pion–pion interactions; as the protons are conceived in this model as $p = (\pi^+\pi^0\vartheta)$, where ϑ is a spectator particle needed for the dynamical generation of quantum numbers of the nucleons. The production of pions in the present scheme occurs as follows: the incident energetic π-mesons in the structure of the projectile proton (nucleon) emits a rho (ϱ)-meson in the interacting field of the pion lying in the structure of the target proton, the ϱ-meson then emits a π-meson and is changed into an omega (ω)-meson, the ω-meson then again emits a π-meson and is transformed once again into a ϱ-meson and thus the process of production of pion secondaries continue in the sequential chain of $\varrho - \omega - \pi$ mesons. The two ends of the diagram contain the baryons exclusively.[23–34]

For $K^+(K^-)$ or $K^0\bar{K}^0$ production the model proposes the following mechanism. One of the interacting pi-mesons emits a rho-mesons; the rho-mesons in its turn emits a ϕ^0-meson and a pi-meson. The pi-meson so produced then again emits ρ and ϕ^0 mesons and the process continues. The ϕ^0 mesons so produced now decays into either K^+K^- or $K^0\bar{K}^0$ pairs. The $\rho - \pi$ chain proceeds in any Feynmann diagram in a line with alternate positions, pushing the ϕ^0 mesons (as producers of K^+K^- or $K^0\bar{K}^0$ pairs) on the sides. This may appear paradoxical as the ϕ^0 production cross-section is generally smaller than the $K\bar{K}$ production cross-section; still the situation arises due to the fact that the ϕ^0 resonances produced in the collision processes will quickly decay into $K\bar{K}$ pairs, for which the number of ϕ^0 will be lower than that of the $K\bar{K}$ pairs. It is assumed that the K^+K^- and $K^0\bar{K}^0$ pairs are produced in equal proportions.[23–34] The entire production process of kaon–antikaons is controlled by jointly the coupling constants, involving $\rho - \pi - \phi$ and $\phi^0 - K^+K^-$ or $\phi^0 - K^0\bar{K}^0$.

Now we describe here the baryon–antibaryon production. According to the SCM mechanism, the decay of the pion secondaries produces baryon–antibaryon pairs in a sequential chain as before. The pions producing baryons–antibaryons pairs are obviously turned into the virtual states. And the proton–antiproton pairs are just a part of these secondary baryon–antibaryon pairs. In the case of baryon–antibaryon pairs it is postulated that protons–antiprotons and neutrons–antineutrons constitute the major bulk and the production of the strange baryons-antibaryons are far less due to the much smaller values of the coupling constants.

It is to be noted that the present model is totally a field-theoretic one and the expressions are derived here from the kinematics of the infinite momentum frame for the inclusive production cross-sections and the average multiplicity values of the various types of secondary pions (of any variety), kaons (of each type) and antiprotons produced in the chain. The details on the derivations of the expressions for inclusive cross-sections, average multiplicities, average transverse momenta, etc.

of pions, kaons and antiprotons for the soft processes are to be obtained now from some of our previous work referenced.[23–34] The underlying assumptions and approximations are also stated therein with regard to the particular cases. The clues to deriving some numerical values used in the standard expressions are given therein. But for analyzing the RHIC-data, we cannot start with the soft production alone; we have to certainly take into account the factors arising out of "hard" (high-p_T) production. And the total inclusive cross-section is obtained by the joint probability of the production amplitude in both the "hard" and the "soft" processes. The following starting expression is one such for production of any variety of secondary pions in PP collisions:

$$E\,\frac{d^3\sigma}{dp^3}\bigg|_{PP\to\pi^- X} = \frac{\mathrm{CRT}}{4\pi}\,\frac{f^2_{\varrho\omega\pi}}{16\pi^2}\,\Psi(x,p_T,s)\,, \tag{1}$$

where CRT is the "constituent rearrangement term" arising out of the partons inside the proton which essentially provides a damping term in terms of a power-law in p_T with an exponent of varying values depending on both the collision process and the specific p_T-range. This part represents physically the basic contribution from the hard (large-p_T) interactions. The other factors in the expression (1) are just the derived results of the structure function for soft PP interaction based on the $\rho-\omega-\pi$ sequential chain model. This indicates the most important soft (small-p_T) contribution to the inclusive cross-section in PP. The exact forms of the expressions of $\Psi(x,p_T,s)$ in Eq. (1) for the various secondaries are to be obtained from Refs. 23–34. It is established that hadrons (baryons and mesons) are composed of few partons. At large transverse momenta in the high energy interaction processes the partons undergo some dissipation losses due to the impact and impulse of the projectile on the target and they suffer some forced shifts of their placements or configurations. The transitions may occur from top-to-top and bottom-to-bottom (H-type diagrams) or cross-wise from top-to-bottom and bottom-to-top (X-type diagrams) or in-between.[28,29] This phenomenon means undesirable loss of energy, in so far as the particle production mechanisms are concerned. This is, again, dependent on the center-of-mass energy of the interactions, i.e. on $\sqrt{s_{NN}}$. This damping term is finally expressed (in terms of p_T for large-p_T domain) in the form $\sim (p_T)^{-4n\theta}$ where $n =$ no. of partons undergoing the rearrangement of position and $\theta =$ a phase term, with maximum value equal to unity and normally is $\ll 1$.[28,29] Denoting $4n\theta$ by N_R, we may express, the value of CRT as $\sim p_T^{-N_R}$, wherein the choice of N_R would depend on the following factors: (i) the specificities of the interacting projectile and target, (ii) the particularities of the secondaries emitted from a specific hadronic interaction and (iii) the magnitude of the momentum transfer for different centrality regions in a specific reaction.

However, the factor $f^2_{\varrho\omega\pi}/4\pi$ in above equation is the coupling strength for $\varrho\omega\pi$ coupling.

The term $\Psi(x,p_T,s)$ is a well-known structure function term for production of pions with x, the Feynman scaling variable; p_T the transverse momenta and

s being the square of the c.m. energy. For small p_T, the form of the structure function[23–34] is

$$\Psi(x, p_T, s) \to \exp(-2.38\langle n_{\pi^-}\rangle_{PP} x) \exp\left(\frac{-26.88 p_T^2}{\langle n_{\pi^-}\rangle_{PP}(1-x)}\right), \tag{2}$$

$$\langle n_{\pi^+}\rangle_{PP} \cong \langle n_{\pi^-}\rangle_{PP} \cong \langle n_{\pi^0}\rangle_{PP} \cong 1.1 s^{1/5}, \tag{3}$$

where $\langle n_{\pi^-}\rangle$ is the average multiplicity of the pion.

Combining Eqs. (1) and (2) for inclusive cross-section for production of pions at high transverse momentum now reduces to

$$E\frac{d^3\sigma}{dp^3}\bigg|_{PP\to\pi^- x} \cong C_{\pi^-} \exp(-2.38\langle n_{\pi^-}\rangle_{PP} x) \frac{1}{p_T^{(N_R^{\pi^-})}} \times \exp\left(\frac{-26.88 p_T^2}{\langle n_{\pi^-}\rangle_{PP}(1-x)}\right), \tag{4}$$

where C_π is the normalization factor which will increase as the inelastic cross-section increases and it is different for different energy region, for example, $|C_\pi| \cong 90$ for intersecting storage ring (ISR) energy region.

Similarly, for kaons of any specific variety (K^+, K^-, K^0 or $\bar{K^0}$) we have

$$E\frac{d^3\sigma}{dp^3}\bigg|_{PP\to K^- x} \cong C_{K^-} \frac{1}{p_T^{(N_R^{K^-})}} \exp(-6.55\langle n_{K^-}\rangle_{PP} x) \exp\left(\frac{-1.33 p_T^2}{\langle n_{K^-}\rangle_{PP}^{3/2}}\right), \tag{5}$$

with $|C_{K^-}| \cong 11.22$ for ISR energies and with

$$\langle n_{K^+}\rangle_{PP} \cong \langle n_{K^-}\rangle_{PP} \cong \langle n_{K^0}\rangle_{PP} \cong \langle n_{\bar{K^0}}\rangle_{PP} \cong 5 \times 10^{-2} s^{1/4}. \tag{6}$$

And for the antiproton production in pp scattering at high energies, the derived expression for inclusive cross-section is

$$E\frac{d^3\sigma}{dp^3}\bigg|_{PP\to\bar{p}x} \cong C_{\bar{p}} \frac{1}{p_T^{(N_R^{\bar{P}})}} \exp(-25.4\langle n_{\bar{p}}\rangle_{PP} x) \exp\left(\frac{-0.66(p_T^2)_{\bar{p}} + {m_{\bar{p}}}^2}{\langle n_{\bar{p}}\rangle_{PP}^{3/2}(1-x)}\right), \tag{7}$$

with $|C_{\bar{p}}| \cong 1.87 \times 10^3$ and $m_{\bar{p}}$ is the mass of the antiprotons. For ultrahigh energies

$$\langle n_{\bar{p}}\rangle_{PP} \cong \langle n_p\rangle_{PP} \cong 2 \times 10^{-2} s^{1/4}. \tag{8}$$

In addition to the statistically equal probability of production of positive, negative and neutral variety of particles, there are some additional modes of production of only the positive particles leading apparently to the nature's favoritism to the positive particles.[27]

The physics behind the observed preference of nature for the production of positive secondary particles on the basis of this model is like this. Protons are composite states of one positive pion, one neutral pion and one spectator particle, identified to be a Majorana spinor from the constraints of the model, which obviously does not take part in the strong interaction processes. Quite naturally, according to this version of the structure of hadrons, antiprotons will consist of one negative

pion, one neutral pion and the same spectator. In addition to what is produced in multiple production of hadrons in the chain, in a somewhat statistical fashion the positive particles may come out from their structural configurations or from inside the hadrons at high energies and especially at large transverse momentum. In PP interactions the positive particles stand equal chances of emission at both extreme vertices of interaction. Hence this contributes to the excess production.

So for all varieties of positive particles (π^+ mesons, K^+ mesons, protons, etc.) there are some extraneous modes of production, as a result of which there is a manifest tendency in nature towards a little excess production of all positive particles. This aspect was treated in a field theoretic manner, in the reference cited above,[27] in some detail. And the excess terms and final forms for them in the field theoretic formulation could be laid down by the following expressions for the varieties of particles like π^+, K^+ mesons and protons:

$$(B_{\pi^+})_{pp} = \frac{4}{3}\, g^2_{p\pi\pi}\, \frac{(P'+K)^2}{[(P'+K)^2 - m_p^2]^2}\, A(\nu, q^2)_\pi \int \frac{d^3k_\pi}{2k_0(2\pi)^3} \exp(-ik_\pi x)\,, \quad (9)$$

$$(B_{K^+})_{pp} = \frac{1}{2}\,(4\pi g^2_{KN\Lambda} + 4\pi g^2_{\Sigma KN})\, \frac{1}{[(P'+K)^2 - m_p^2]^2}\, A(\nu, q^2)_K \times \int \frac{d^3k_K}{2k_0(2\pi)^3} \exp(-ik_K x)\,, \quad (10)$$

$$(B_p)_{pp} = \frac{4\pi g^2_{NN\pi}}{[(P'+K)^2 - m_p^2]^2}\, A(\nu, q^2)_{p_s} \int \frac{d^3k_p}{2(2\pi)^3} \exp(-ik_p x)\,, \quad (11)$$

where the symbols have their contextual connotation with the following hints to the physical reality of extraneous π^+, K^+ and protons productions as nonleading secondaries. The first parts of the above equations (Eqs. (9)–(11)), contain the coupling strength parameters, the second terms of the above equations are just the propagator for excited nucleons. The third terms represent the common multiparticle production amplitudes along with extraneous production modes and the last terms indicate simply the phase space integration terms on the probability of generation of a single π^+, K^+ and proton, respectively. These expressions are to be calculated by the typical field-theoretical techniques and are to be expressed — if and when necessary — in terms of the relevant variable and/or measured observables.

2.2. *Transition from NN to AA collisions: The flyover at high energies*

In order to build the bridge between nucleon–nucleon interactions and the nucleus–nucleus collisions, we proceed in the path suggested by Wong.[35] As a first step in the process, let us consider a nuclear reaction $A + B \to C + X$, where A and B are projectile and target nucleus, respectively. In such a collision, for the impact parameter b, we assume that there are $n'(b)$ number of inelastic nucleon–nucleon collisions. Each collision contributes to the production of particles. If all the collisions

contribute in the same way, the production cross-section $E\frac{d^3\sigma}{dp^3}$ for the nucleus–nucleus collisions would just be $n'(b)$ times the production cross-section $E\frac{d^3\sigma}{dp^3}$ for the nucleon–nucleon collisions.

However, the contribution from all of the collisions are not the same. One can envisage that in a nucleus–nucleus collision, those nucleon–nucleon collisions which occur later in the process contribute less than those collisions from earlier collisions, because of the stopping of the baryons of one nucleus as they go through the other nucleus. The degree of stopping depends on the thickness of the projectile and the target nuclei. One observes that there are greater degradation of the energies of the colliding nucleons in central collisions as compared to peripheral ones. The slight decrease of the transverse energy per collision with the decrease of the impact parameter is an indication of the effect of energy degradation, when nucleons of the projectile-nucleus traverse through the target-nucleus. So, in fine, for heavy nuclei and high energy nuclear collisions which entail involvement of large number of nucleons and multiple binary collisions, the role of the energy degradation factor is certainly not negligible; and the energy degradation term as presented by Wong[35] would have its impact on the number of wounded nucleons and thus also on $\langle N_{\text{part}}\rangle$.[36] If and when one uses this stopping effect to the first power in the thickness of the projectile and of the target-nucleus, the resultant effect of energy degradation should lead to a reduction factor of the form $1/[1 + a'(A^{1/3} + B^{1/3})]$. Thus, the relationship between the production cross-section for nucleus–nucleus interactions and that for nucleon–nucleon collisions is given by

$$E\frac{d^3\sigma}{dp^3}dy\bigg|_{AB} \cong \frac{n'(b)}{1 + a'(A^{1/3} + B^{1/3})}\, E\,\frac{d^3\sigma}{dp^3}\bigg|_{pp}, \tag{12}$$

where a' is a parameter that is to be chosen. For the present work the chosen values of a' lie in the range $\sim$0.09–0.15.[35]

Using Woods–Saxon nuclear density distribution we obtain the expression for the average number of wounded nucleons as given by[37]

$$n' = \frac{A\sigma_B + B\sigma_A}{\sigma_{AB}}, \tag{13}$$

where σ_A is the nucleon (proton)–nucleus (A) production cross-section, σ_B is the inelastic nucleon (proton)–nucleus (B) production cross-section and σ_{AB} is the inelastic production cross-section for the collision of nucleus A and nucleus B. The values of σ_{AB}, σ_A, σ_B are worked here out in a somewhat heuristic manner by the following formula:[38]

$$\sigma_{AB}^{\text{inel}} = \sigma_0\Big(A_{\text{projectile}}^{1/3} + A_{\text{target}}^{1/3} - \delta\Big)^2 \tag{14}$$

with $\sigma_0 = 68.8$ mb, $\delta = 1.32$. Thus one obtains from Eq. (14) $\sigma_{\text{Au Au}}^{\text{inel}} \simeq 6.84$ barn. The values of σ_A and σ_B are also computed here by using Eq. (14) and taking unity for the mass number value of one of the nuclei. Obviously this is both an approximate and a shortcut method. However, the nuclear density expressions would be

necessary for the rigorous calculations (demanding simulations) on the values of all the terms, viz., σ_{AB}, σ_A and σ_B.

Now by combining all the equations from Eqs. (12) to (14) and applying them to Eq. (12), we finally arrive at

$$E\,\frac{d^3\sigma}{dp^3}\bigg|_{AB} \simeq \frac{(A\sigma_B + B\sigma_A)}{\sigma_{AB}}\,\frac{1}{1+a'(A^{1/3}+B^{1/3})}\,E\,\frac{d^3\sigma}{dp^3}\bigg|_{pp}. \tag{15}$$

For the present purpose and for practical reasons, we shall use here the undernoted relation to calculate the transverse momentum distributions for different secondaries at different centralities in a particular reaction

$$\left(\frac{1}{\sigma_{\text{in}}}\right) E\,\frac{d^3\sigma}{dp^3} \cong \frac{1}{2\pi p_T}\,\frac{d^2N}{dp_T\,dy}. \tag{16}$$

3. Measured Data versus Model-Based Results

Here we deal with some of the secondaries-production data available from the Brookhaven RHIC of Au + Au collisions at $\sqrt{s_{NN}} = 200$ GeV[39] and try to interpret them theoretically with the help of the modified SCM for the AA collisions. In the first three subsections the pions, kaons and antiproton–protons production are taken into account. The production of different secondaries in minimum-bias, central and peripheral-reaction are considered in the next subsection and the last subsection deals with the ratio-behaviors for the pions, kaons and the baryons.

3.1. *Pion production*

Using Eqs. (3), (4), (15) and (16) we arrive at the expression for transverse momentum distribution of negative pions produced in the gold–gold collisions at $\sqrt{s_{NN}} =$ 200 GeV at RHIC:

$$\frac{1}{2\pi p_T}\,\frac{d^2N}{dp_T\,dy}\bigg|_{\text{Au + Au}\to\pi^- + X} = (a)_{\pi^-}\,\frac{1}{p_T^{(N_R^{\pi^-})}}\exp(-0.54p_T^2), \tag{17}$$

where $(a)_{\pi^-}$ has given by the undernoted relation:

$$(a)_{\pi^-} \equiv C_{\pi^-}\,\frac{(A\sigma_B + B\sigma_A)}{\sigma_{AB}}\,\frac{1}{1+a'(A^{1/3}+B^{1/3})}\exp(-2.38\langle n_{\pi^-}\rangle_{PPX}).$$

The experimental results for the production of π^- at different centralities (from 0–5% to 80–92%) are taken from the PHENIX group[39] and they are plotted in Figs. 1 and 2 against p_T[GeV/c]. The solid lines in those figures show the theoretical SCM results. The values of $(a)_{\pi^-}$ of Eq. (17) for different centrality regions are taken from Fig. 5. The $N_R^{\pi^-}$'s of Eq. (17) are functions of both the centrality of the bins and of energy. It appears due to the constituent rearrangement (CR) in the structure of basic nucleon–nucleon collisions at high energies and large transverse momenta; and its values for negative pions are given in Table 1.

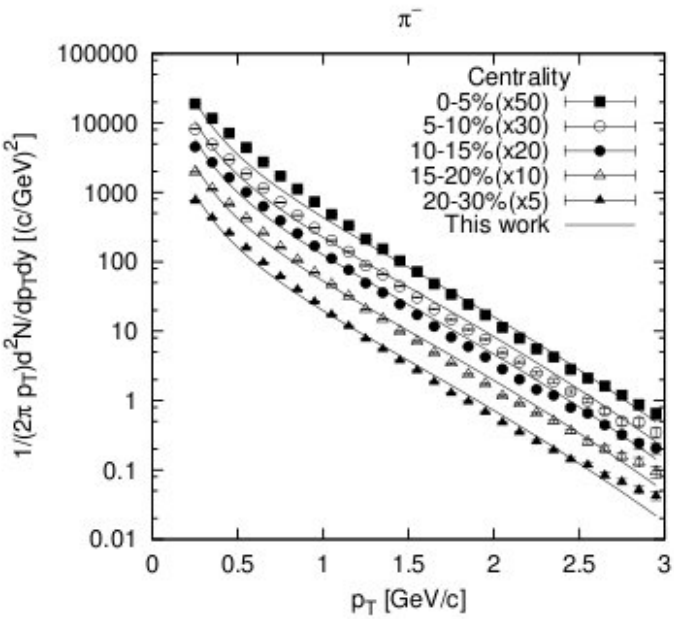

Fig. 1. Centrality dependence of the p_T distribution for π^- for different centralities from 0–30% in Au Au collisions at $\sqrt{s_{NN}} = 200$ GeV.[39] The lines show the theoretical SCM calculations.

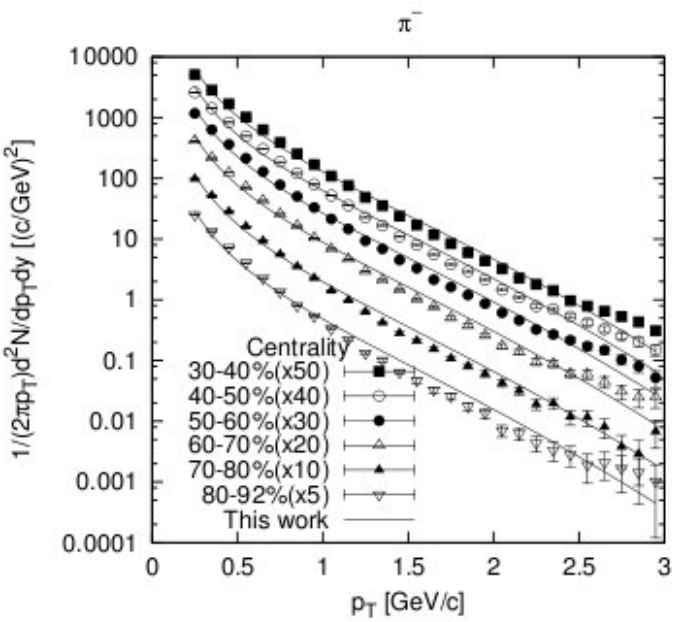

Fig. 2. Centrality dependence of the p_T distribution for π^- for different centralities from 30–92% in Au Au collisions at $\sqrt{s_{NN}} = 200$ GeV.[39] The lines show the theoretical SCM calculations.

Table 1. Values of $N_R^{\pi^-}$ and $N_R^{\pi^+}$ for different centrality regions.

Centrality	0–5%	5–10%	10–15%	15–20%	20–30%
$N_R^{\pi^-}$	2.406	2.409	2.412	2.419	2.435
$N_R^{\pi^+}$	2.419	2.432	2.433	2.446	2.450
30–40%	40–50%	50–60%	60–70%	70–80%	80–92%
2.442	2.473	2.504	2.534	2.559	2.595
2.466	2.485	2.524	2.561	2.588	2.616

In order to arrive at the transverse momentum distribution of π^+, one has to consider the Eq. (9) along with Eqs. (3), (4), (15) and (16). For excess π^+ production, a factor represented by $(1+\alpha_\pi p_T^\pi)$ is to be operated on $\frac{1}{2\pi p_T}\frac{d^2N}{dp_T dy}\big|_{\mathrm{Au+Au}\to\pi^-+X}$ as an multiplier.[27] Combining the multiplying factor and expression (17) we finally obtain

$$\frac{1}{2\pi p_T}\frac{d^2N}{dp_T dy}\bigg|_{\mathrm{Au+Au}\to\pi^++X} = (a)_{\pi^+}\frac{1}{p_T^{(N_R^{\pi^+})}}\exp(-0.54p_T^2), \tag{18}$$

with

$$(a)_{\pi^+} = (1+0.044p_T^\pi)(a)_{\pi^-}\,. \tag{19}$$

As previously stated, the exponents N_R of p_T would depend on the following factors: (i) the specificities of the interacting projectile and target, (ii) the particularities of the secondaries emitted from a specific hadronic interaction and (iii) the magnitude of the momentum transfer for different centrality regions in a specific reaction. Thus, the values of $N_R^{\pi^+}$ for different centralities differ from that of $N_R^{\pi^-}$, and are shown in Table 1. The experimental results for the π^+ productions[39] for different centralities ranging from 0–5% to 80–92% are plotted in Figs. 3 and 4 respectively. The solid lines in those figures show the theoretical fits. The values of $(a)_{\pi^+}$ for different centrality region are taken from Fig. 6.

3.2. *Kaon production*

With the help of the Eqs. (5), (6), (15) and (16), the expression for the transverse momentum distribution for K^- in Au Au collisions at $\sqrt{s_{NN}} = 200$ GeV at RHIC is given by

$$\frac{1}{2\pi p_T}\frac{d^2N}{dp_T dy}\bigg|_{\mathrm{Au+Au}\to K^-+X} = (a)_{K^-}\frac{1}{p_T^{N_R^{K^-}}}\exp(-0.65p_T^2)\,. \tag{20}$$

Here the $(a)_{K^-}$ is given by

$$(a)_{K^-} \equiv C_{K^-}\frac{(A\sigma_B + B\sigma_A)}{\sigma_{AB}}\frac{1}{1+a'(A^{1/3}+B^{1/3})}\exp(-6.55\langle n_{K^-}\rangle_{PP}x)\,.$$

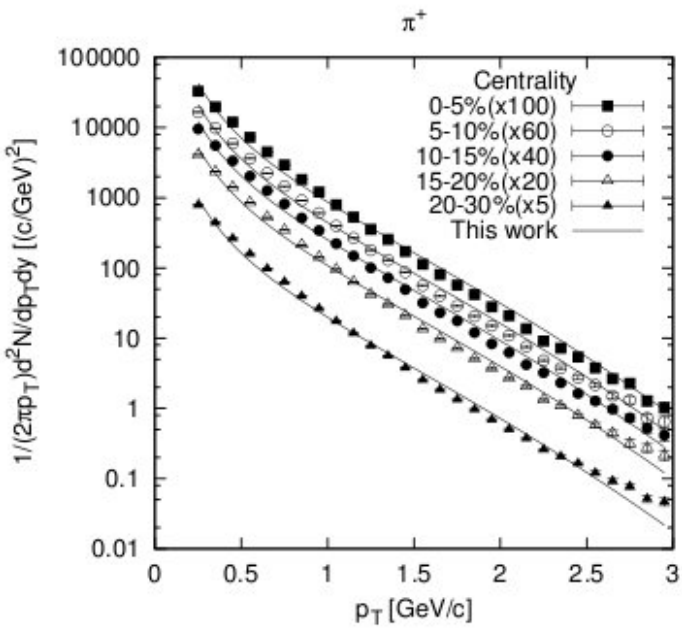

Fig. 3. Centrality dependence of the p_T distribution for π^+ for different centralities from 0–30% in Au Au collisions at $\sqrt{s_{NN}} = 200$ GeV.[39] The lines show the theoretical SCM calculations.

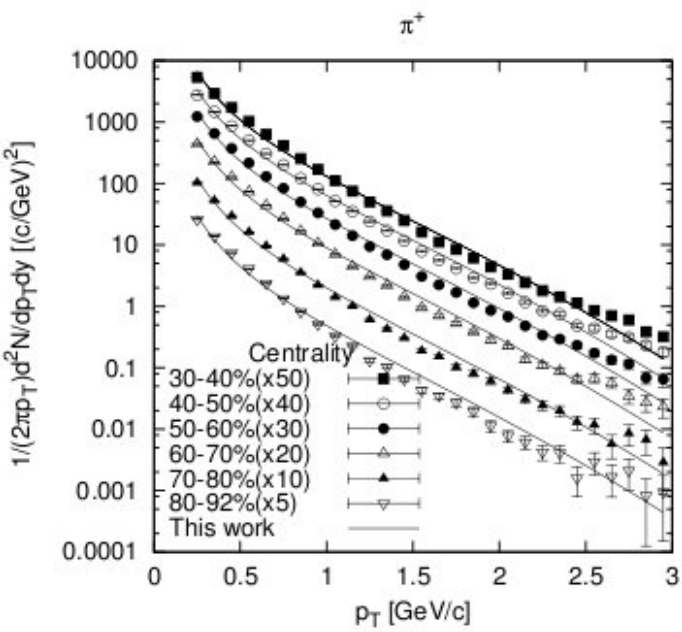

Fig. 4. Centrality dependence of the p_T distribution for π^+ for different centralities from 30–92% in Au Au collisions at $\sqrt{s_{NN}} = 200$ GeV.[39] The lines show the theoretical SCM calculations.

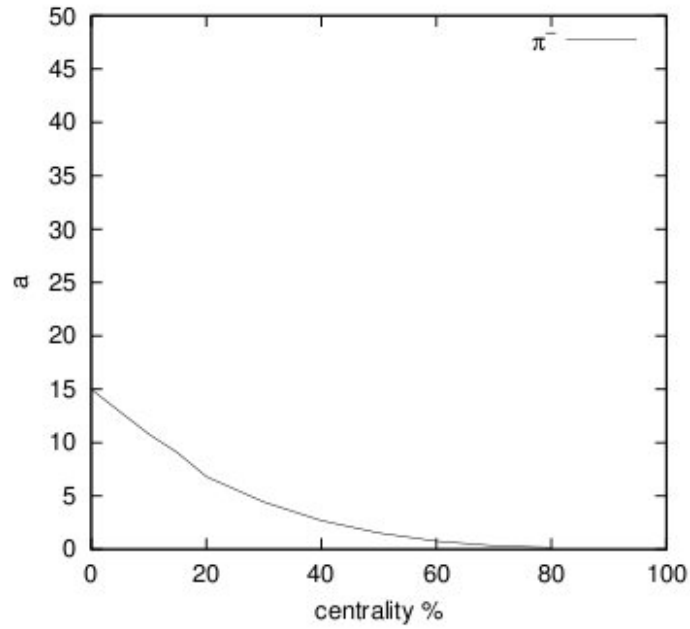

Fig. 5. Centrality dependence of the a_{π^-} distribution for π^- for different centralities.

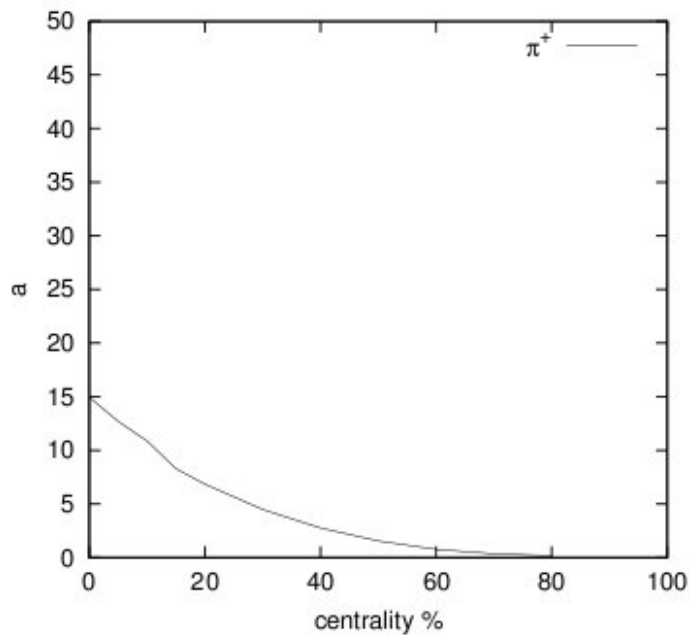

Fig. 6. Centrality dependence of the a_{π^+} distribution for π^+ for different centralities.

Table 2. Values of $N_R^{K^-}$ and $N_R^{K^+}$ for different centrality regions.

Centrality	0–5%	5–10%	10–15%	15–20%	20–30%
$N_R^{K^-}$	1.583	1.591	1.593	1.614	1.636
$N_R^{K^+}$	1.622	1.633	1.634	1.638	1.676
30–40%	40–50%	50–60%	60–70%	70–80%	80–92%
1.691	1.728	1.842	1.894	2.048	2.107
1.692	1.786	1.871	1.940	2.047	2.110

The experimental results are taken from the PHENIX group[39] and they are plotted in Figs. 7 and 8. Figure 7 deals with 0–5% to 20–30% centrality regions whereas Fig. 8 gives 30–40% to 80–92% centrality regions. The solid lines in those figures show the SCM results. The values of $(a)_{K^-}$ for different centrality region are taken from the Fig. 11. The values of $N_R^{K^-}$ of Eq. (20) for different centralities are shown in Table 2.

Adopting the above procedure, as we indicated for the production of positive pions, we obtain for the transverse momentum distribution of K^+ a multiplicative factor $\sim (1 + \alpha_K p_T^K)$ to be operated on $\frac{1}{2\pi p_T}\frac{d^2N}{dp_T dy}\big|_{\mathrm{Au+Au}\to K^-+X}$.[27] Combining the multiplying factor and expression (20) we finally obtain

$$\frac{1}{2\pi p_T}\frac{d^2N}{dp_T dy}\bigg|_{\mathrm{Au+Au}\to K^+ + X} = (a)_{K^+}\frac{1}{p_T^{N_R^{K^+}}}\exp(-0.65p_T^2) \tag{21}$$

with

$$(a)_{K^+} = (1 + 0.082p_T^K)(a)_{K^-}\,. \tag{22}$$

The values of $N_R^{K^+}$ for different centralities are also shown in Table 2. The experimental results[39] for the production of K^+ of different centralities are plotted in Figs. 9 and 10. The solid lines in those figures show the theoretical fits. The values of $(a)_{K^+}$ for different centrality region are plotted in Fig. 12.

3.3. *Antiproton–proton production*

With the help of the Eqs. (7), (8), (15) and (16), the expression for the transverse momentum distribution for antiprotons in AuAu collisions at energy $\sqrt{s_{NN}} = 200$ GeV at RHIC is given by

$$\frac{1}{2\pi p_T}\frac{d^2N}{dp_T dy}\bigg|_{\mathrm{Au+Au}\to \bar{p}+X} = (a)_{\bar{p}}\frac{1}{p_T^{N_R^{\bar{p}}}}\exp(-0.28p_T^2)\,. \tag{23}$$

The $(a)_{\bar{p}}$ of the above equation can be written as

$$(a)_{\bar{p}} \equiv C_{\bar{p}}\frac{(A\sigma_B + B\sigma_A)}{\sigma_{AB}}\frac{1}{1 + a'(A^{1/3} + B^{1/3})}\exp(-25.4\langle n_{\bar{p}}\rangle_{PP}x)\,.$$

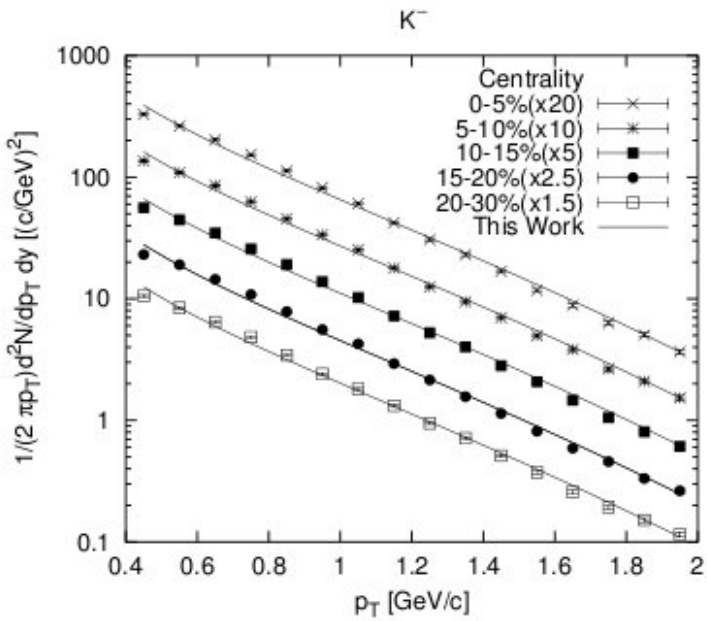

Fig. 7. Plots for centrality dependence of the p_T distribution of K^- for different centralities from 0–30% in Au Au collisions at $\sqrt{s_{NN}} = 200$ GeV.[39] The solid lines show the theoretical fits.

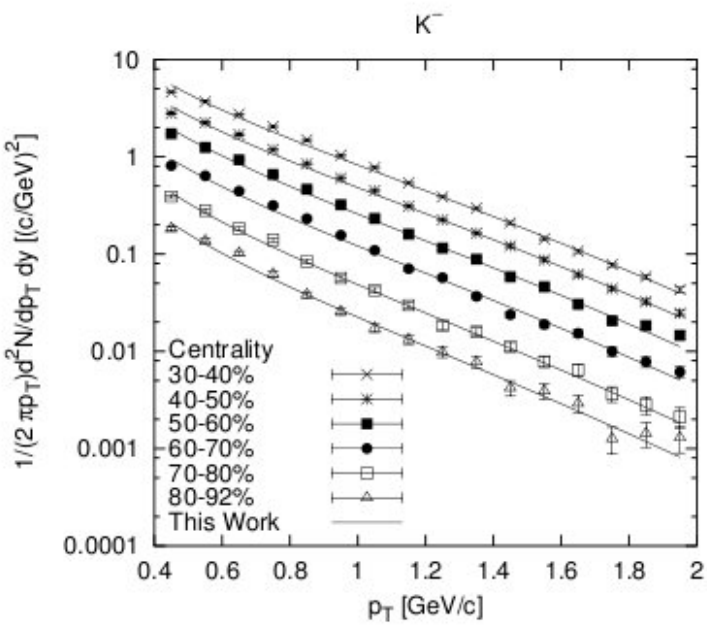

Fig. 8. Plots for centrality dependence of the p_T distribution for K^- for different centralities from 30–92% in Au Au collisions at $\sqrt{s_{NN}} = 200$ GeV.[39] The solid lines show the theoretical fit.

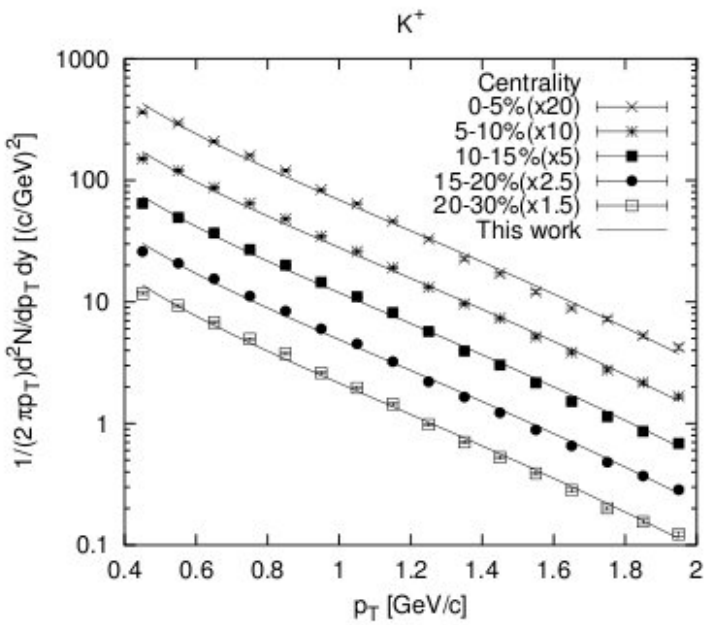

Fig. 9. Plots for centrality dependence of the p_T distribution for K^+ for different centralities from 0–30% in Au Au collisions at $\sqrt{s_{NN}} = 200$ GeV.[39] The solid lines show the theoretical fits.

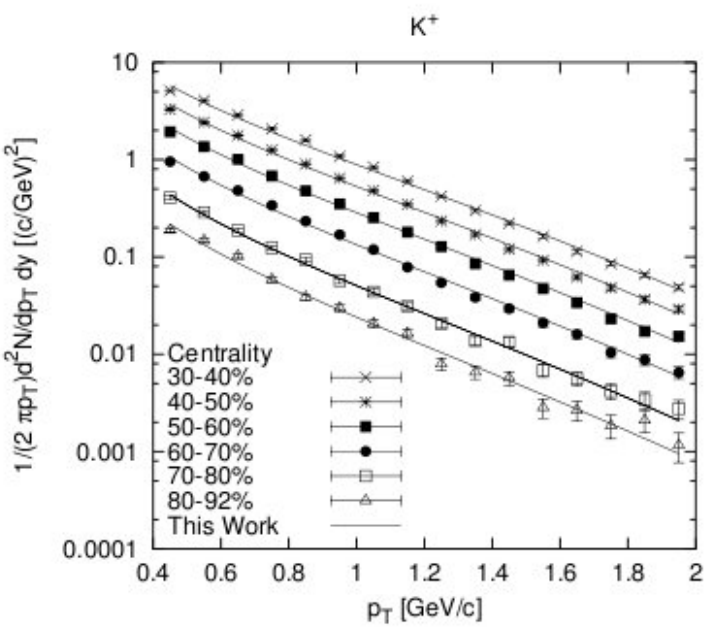

Fig. 10. Plots for centrality dependence of the p_T distribution for K^+ for different centralities from 30–92% in Au Au collisions at $\sqrt{s_{NN}} = 200$ GeV.[39] The solid lines show the theoretical fits.

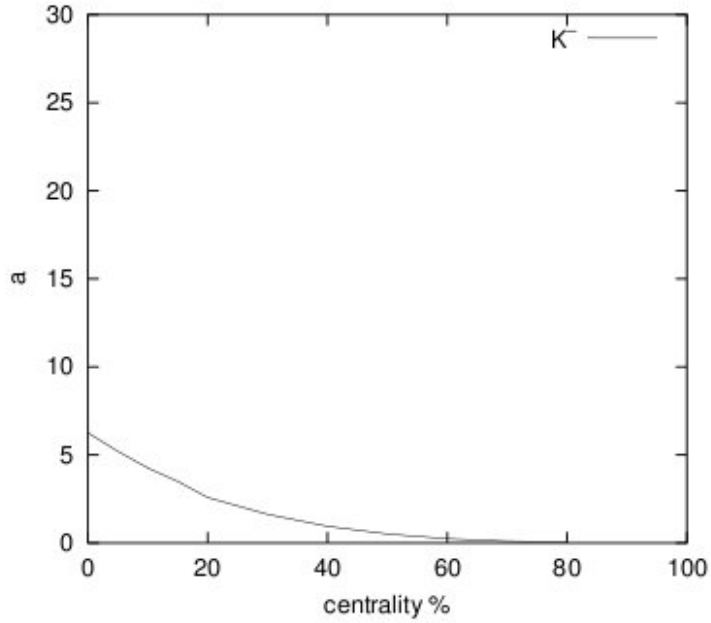

Fig. 11. Centrality dependence of the a_{K^-} distribution for K^- for different centralities.

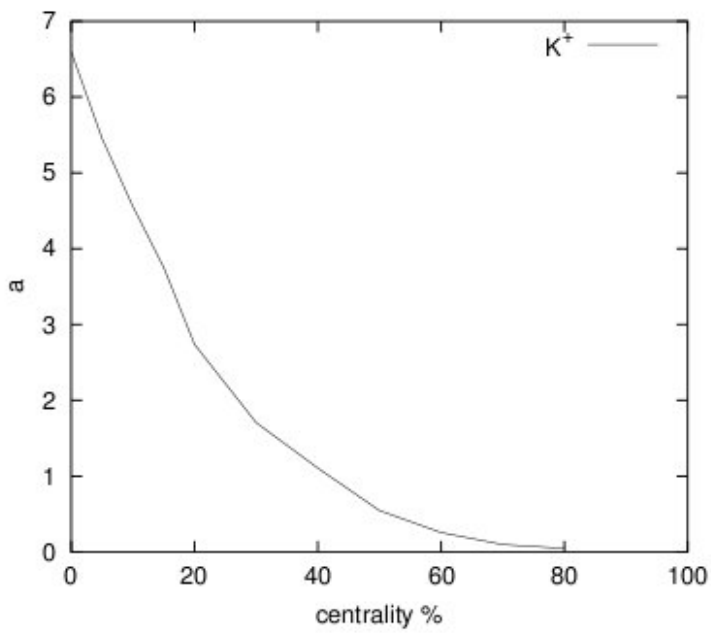

Fig. 12. Centrality dependence of the a_{K^+} distribution for K^+ for different centralities.

Table 3. Values of $N_R^{\bar{p}}$ and N_R^{p} for different centrality regions.

Centrality	0–5%	5–10%	10–15%	15–20%	20–30%
$N_R^{\bar{p}}$	1.894	1.910	1.911	1.933	2.037
N_R^{p}	1.938	1.953	1.959	1.969	2.045
30–40%	40–50%	50–60%	60–70%	70–80%	80–92%
2.117	2.207	2.361	2.558	2.654	2.936
2.109	2.150	2.339	2.518	2.652	2.978

The experimental results for the production of antiproton productions are taken from the PHENIX group[39] and they are plotted against p_T in Figs. 13 and 14 for different centralities. The solid lines in those figures show the theoretical results (Eq. (23)). The values of $(a)_{\bar{p}}$ for different centrality region are taken from Fig. 17. The values of $N_R^{\bar{p}}$ for different centralities are shown in Table 3.

For the production of protons, using Eqs. (11) and (23), we obtain for the transverse momentum distribution of p a multiplicative factor $\sim (1 + \alpha_p p_T^p)$ to be operated on $\frac{1}{2\pi p_T}\frac{d^2N}{dp_T dy}$. Combining the multiplying factor and expression (23) we finally obtain

$$\left.\frac{1}{2\pi p_T}\frac{d^2N}{dp_T dy}\right|_{\mathrm{Au+Au}\to p+X} = (a)_p \frac{1}{p_T^{N_R^p}} \exp(-0.28p_T^2) \tag{24}$$

with

$$(a)_p = (1 + 0.32p_T^K)(a)_{\bar{p}}\,. \tag{25}$$

The exponents, N_R^p for different centralities are given in Table 3. The experimental results[39] for different centralities are plotted in Figs. 15 and 16. The solid lines in those figures show the theoretical fits for the production of protons in relativistic heavy ion collisions of gold–gold at RHIC with energy $\sqrt{s_{NN}} = 200$ GeV. The values of $(a)_p$ for different centrality region are plotted in Fig. 18 and these values are taken to draw the theoretical plots in Figs. 15 and 16.

3.4. *The minimum bias, central and peripheral reactions*

In this section, we specifically deal with the production of different secondary particles in minimum bias, most central (0–5%) and peripheral collisions (60–92%). We would like to compare here the nature of production of the secondary particles like pions, kaons and baryons by plotting them in the same scale against the transverse momenta p_T. The experimental data are taken from PHENIX group[39] for the reaction $\mathrm{Au} + \mathrm{Au} \to C + X$ at $\sqrt{s_{NN}} = 200$ GeV. Figure 19 deals with π^-, K^- and $\bar{p}$ at minimum bias conditions. The lines in Fig. 19 give the SCM-based calculated results for π^-, K^- and $\bar{p}$ by taking the help of Eqs. (17), (20) and (23). The values of a and N_R for different negative secondaries produced in minimum bias conditions are given in Table 4.

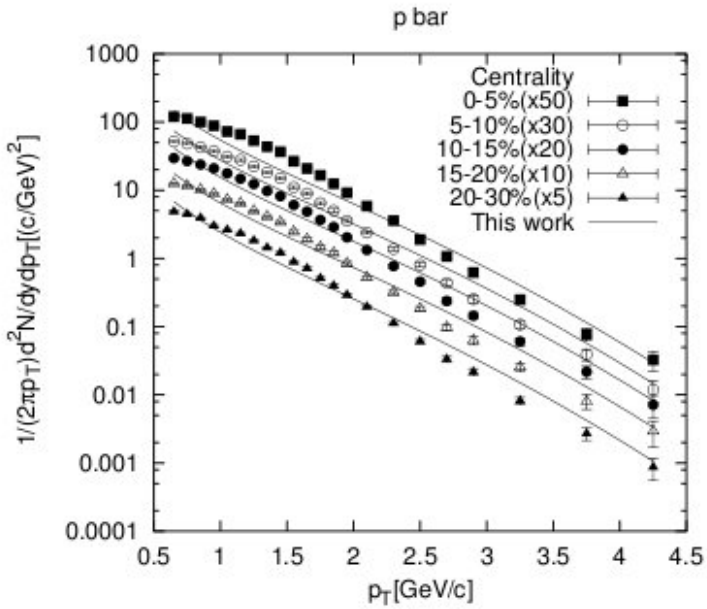

Fig. 13. Centrality dependence of the p_T distribution for $\bar{p}$ for different centralities from 0–30% in Au Au collisions at $\sqrt{s_{NN}} = 200$ GeV.[39] The lines show the theoretical SCM calculations.

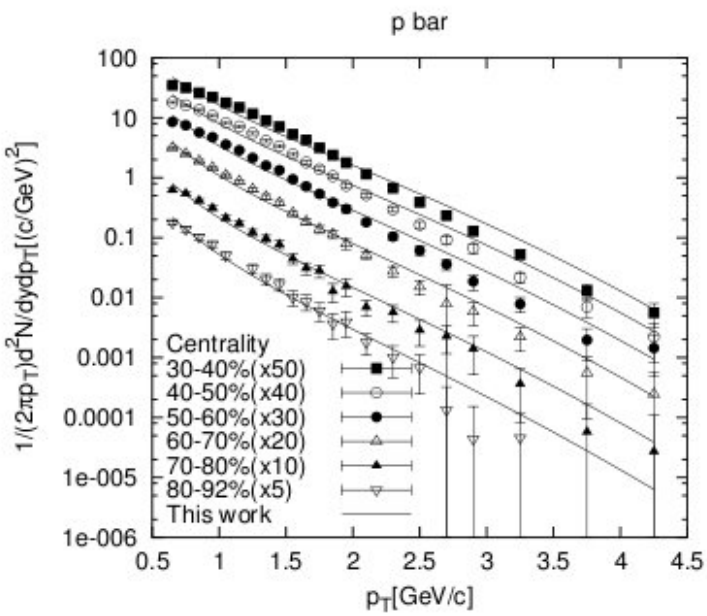

Fig. 14. Centrality dependence of the p_T distribution for $\bar{p}$ for different centralities from 30–92% in Au Au collisions at $\sqrt{s_{NN}} = 200$ GeV.[39] The lines show the theoretical SCM calculations.

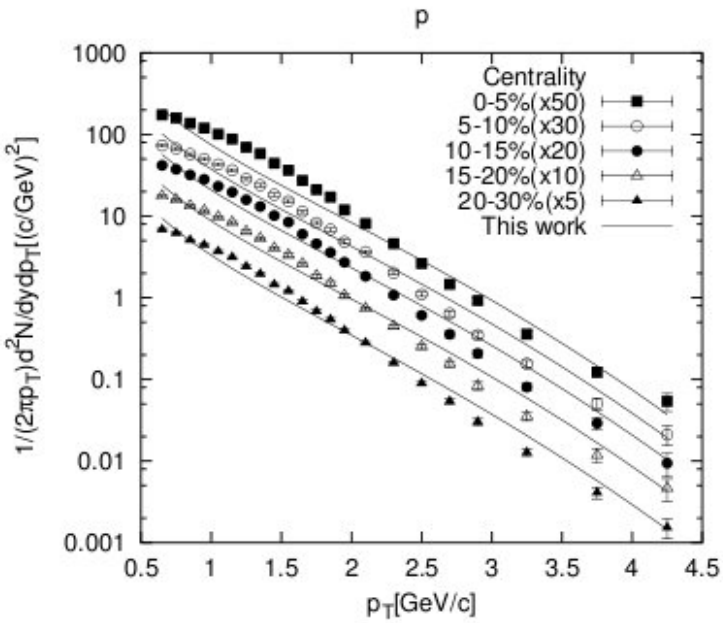

Fig. 15. Centrality dependence of the p_T distribution for p for different centralities from 0–30% in Au Au collisions at $\sqrt{s_{NN}} = 200$ GeV.[39] The lines show the theoretical SCM calculations.

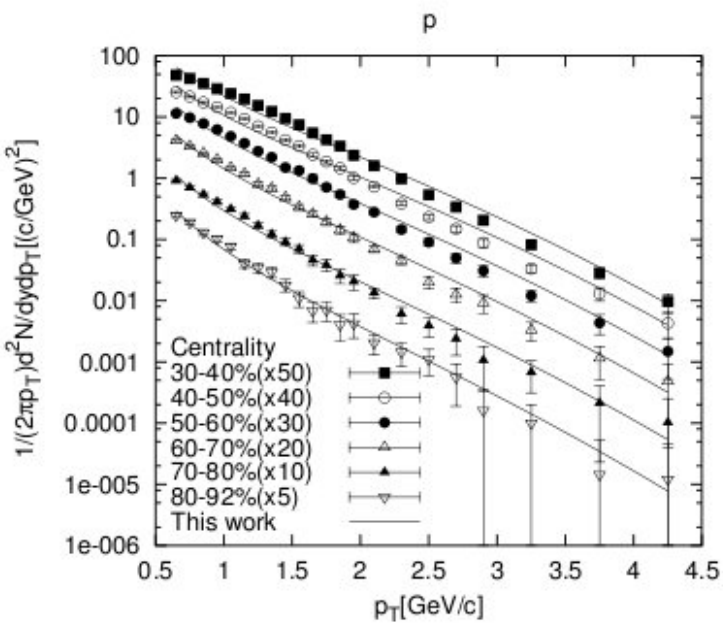

Fig. 16. Centrality dependence of the p_T distribution for p for different centralities from 30–92% in Au Au collisions at $\sqrt{s_{NN}} = 200$ GeV.[39] The line shows the theoretical SCM calculations.

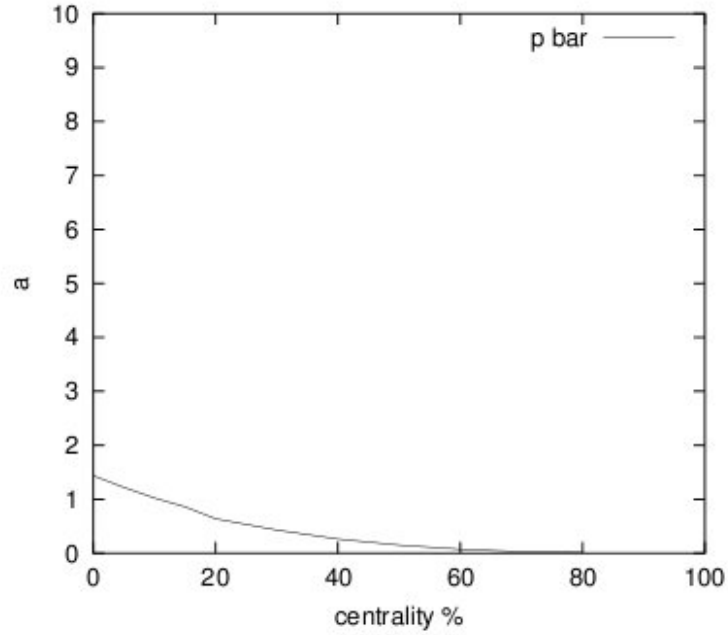

Fig. 17. Centrality dependence of the $a_{\bar{p}}$ distribution for $\bar{p}$ for different centralities.

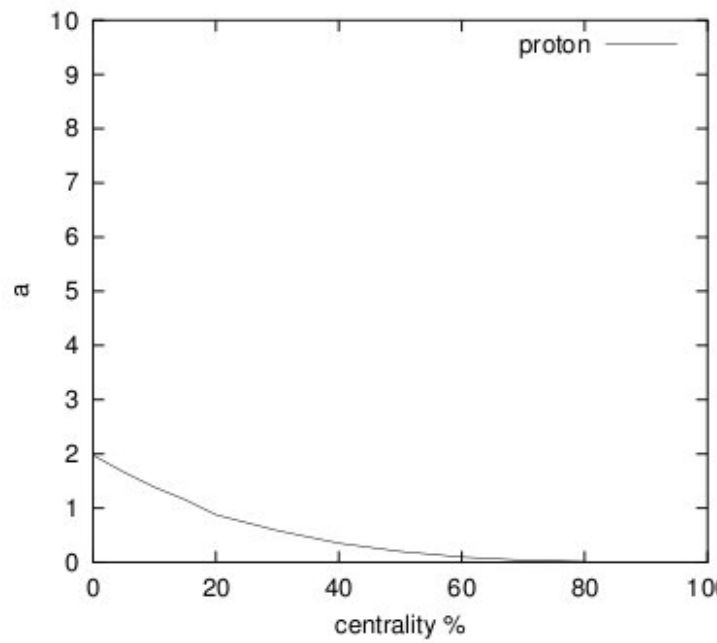

Fig. 18. Centrality dependence of the a_p distribution for p for different centralities.

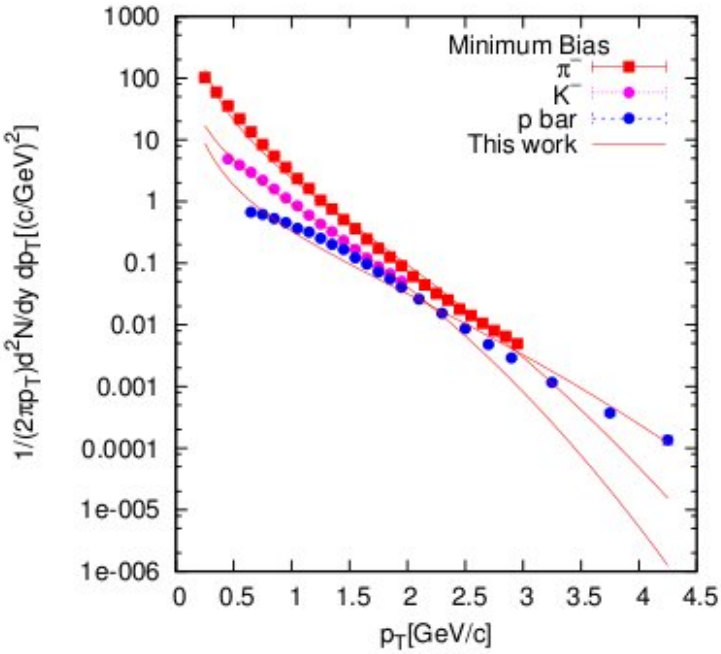

Fig. 19. Transverse momentum distributions for π^-, K^-, $\bar{p}$ in Au + Au collisions at $\sqrt{s_{NN}} =$ 200 GeV. The figure show p_T spectra for the minimum bias collisions. The line shows the SCM-based results for different secondaries.

Table 4. Values of a and N_R for different secondaries in minimum bias regions.

$a_{\pi-}$	a_{K-}	$a_{\bar{p}}$	$a_{\pi+}$	a_{K+}	a_p
3.869	1.760	0.439	3.951	1.876	0.599
$N_R^{\pi^-}$	$N_R^{K^-}$	$N_R^{\bar{p}}$	$N_R^{\pi^+}$	$N_R^{K^+}$	N_R^p
2.599	1.667	2.174	2.606	1.692	2.169

For the productions of π^+, K^+ and p in minimum bias reactions, Eqs. (18), (19), (21), (22), (24) and (25) are taken into account. The values of a and N_R for different positive secondaries are also given in Table 4. Figure 20 depicts the productions of π^+, K^+ and p in minimum bias. Data are taken from the PHENIX for Au Au collisions at $\sqrt{s_{NN}} = 200$ GeV. Lines show the theoretically calculated results.

Similarly, Figs. 21 and 22 show the productions of negative and positive secondaries in most central reactions (0–5%) at gold–gold collisions at energy $\sqrt{s_{NN}} = 200$ GeV. The lines show the theoretical results, wherein the points show the experimental findings at RHIC. The values for a's and N_R's for the case of

Table 5. Values of a and N_R for different secondaries in central (0–5%) regions.

$a_{\pi-}$	a_{K-}	$a_{\bar{p}}$	$a_{\pi+}$	a_{K+}	a_{p}
14.991	6.252	1.472	14.937	6.599	1.472
$N_R^{\pi^-}$	$N_R^{K^-}$	$N_R^{\bar{p}}$	$N_R^{\pi^+}$	$N_R^{K^+}$	N_R^{p}
2.406	1.583	1.894	2.419	1.622	1.938

Table 6. Values of a and N_R for different secondaries in peripheral (60–92%) regions.

$a_{\pi-}$	a_{K-}	$a_{\bar{p}}$	$a_{\pi+}$	a_{K+}	a_{p}
0.417	0.130	0.038	0.416	0.138	0.038
$N_R^{\pi^-}$	$N_R^{K^-}$	$N_R^{\bar{p}}$	$N_R^{\pi^+}$	$N_R^{K^+}$	N_R^{p}
2.590	1.972	2.624	2.642	1.997	2.624

central collisions for different secondaries are given in Table 5. Figures 23 and 24 give the productions of negative and positive secondaries in peripheral reactions (60–92%), respectively. The theoretical curves are obtained with the help of above-mentioned equations. The values of a and N_R for peripheral reactions for different secondaries are given in Table 6.

3.5. *The ratio behaviors for different secondaries*

3.5.1. *The π^-/π^+ ratios*

The π^-/π^+ ratios equations for central (0–5%) and peripheral reactions (60–92%) in the light of SCM are directly obtained from the expressions for the theoretical plots of Figs. 21–24 and they are given by the undernoted relations

$$\left.\frac{\pi^-}{\pi^+}\right|_{\text{central}} = 1.003 p_T^{0.027}, \tag{26}$$

$$\left.\frac{\pi^-}{\pi^+}\right|_{\text{peripheral}} = 1.002 p_T^{0.052}. \tag{27}$$

The curves are drawn in Figs. 25 and 26 against the experimental background. Data are taken from the PHENIX collaboration.[39]

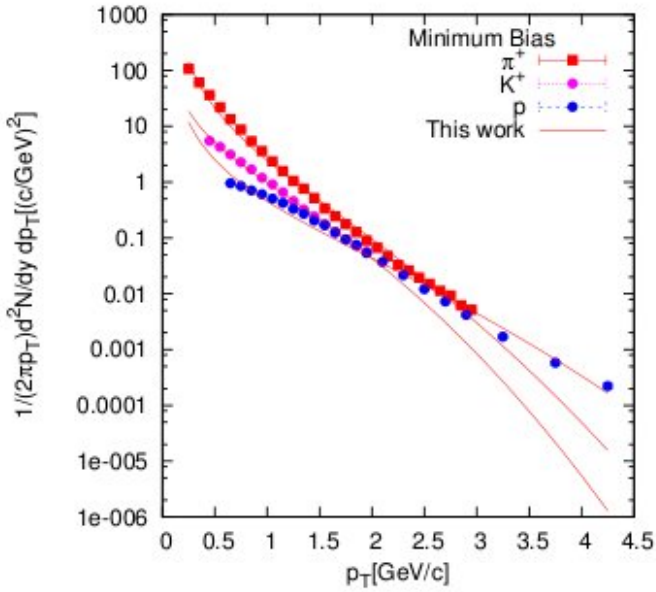

Fig. 20. Transverse momentum distributions for π^+, K^+, p in Au + Au collisions at $\sqrt{s_{NN}} =$ 200 GeV. The figure show p_T spectra for the minimum bias collisions. The line shows the SCM-based results.

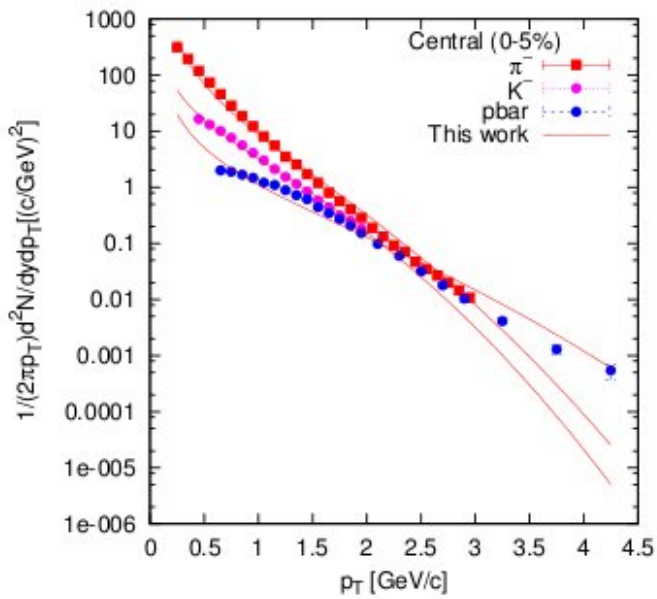

Fig. 21. Transverse momentum distributions for π^-, K^-, $\bar{p}$ in Au + Au collisions at $\sqrt{s_{NN}} =$ 200 GeV. The figure show p_T spectra for the most central collisions (0–5%). The lines show the SCM-based results for different secondaries.

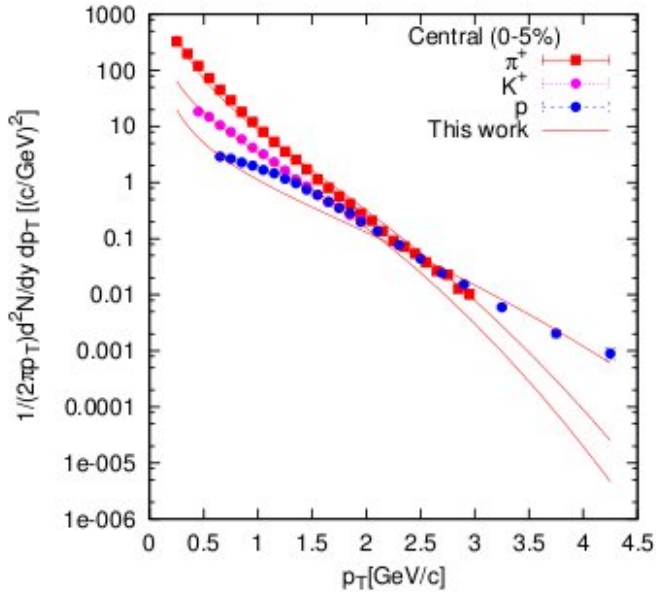

Fig. 22. Transverse momentum distributions for π^+, K^+, p in Au + Au collisions at $\sqrt{s_{NN}} =$ 200 GeV. The figure show p_T spectra for the most central collisions. The lines show the SCM-based results.

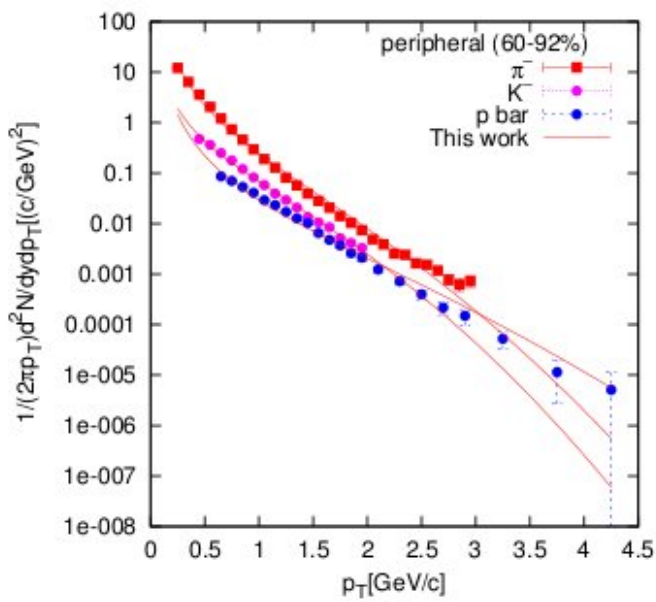

Fig. 23. Transverse momentum distributions for π^-, K^-, $\bar{p}$ in Au + Au collisions at $\sqrt{s_{NN}} =$ 200 GeV. The figure show p_T spectra for the peripheral collisions (60–92%). The lines show the SCM-based results for different secondaries.

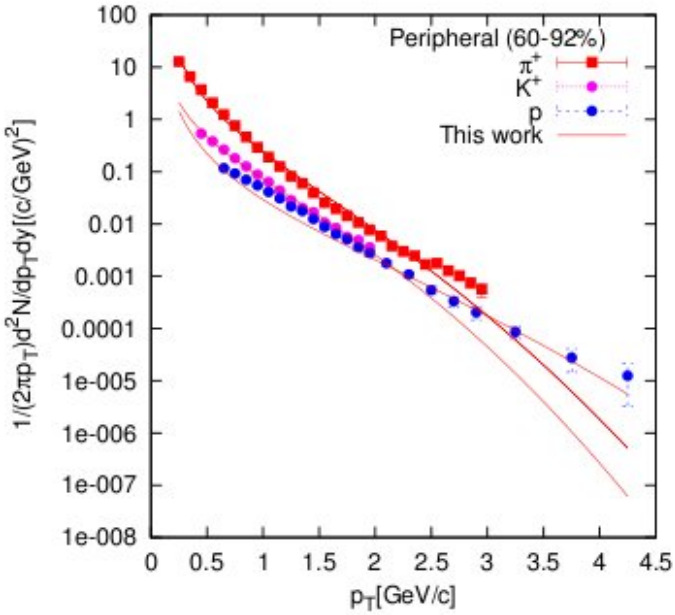

Fig. 24. Transverse momentum distributions for π^-, K^-, $\bar{p}$ in Au + Au collisions at $\sqrt{s_{NN}} =$ 200 GeV. The figure show p_T spectra for the peripheral collisions. The lines show the SCM-based results.

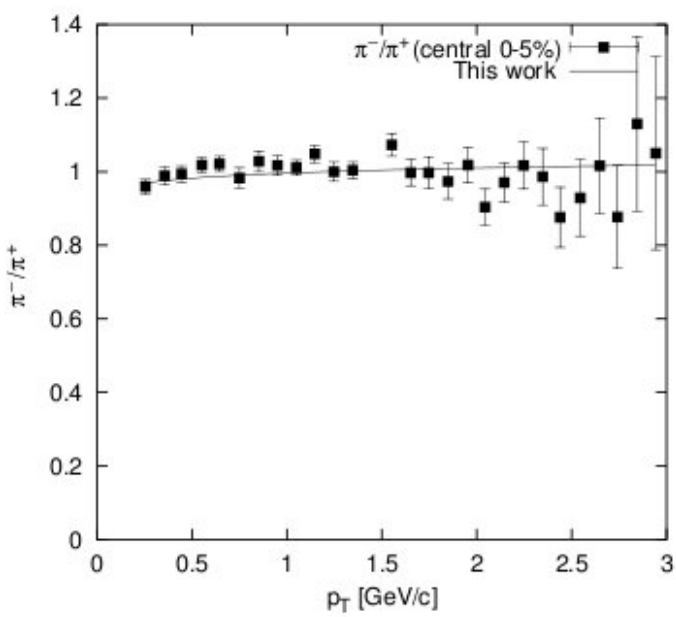

Fig. 25. The π^-/π^+ ratio behaviors at the central reaction (0–5%). Data are taken from PHENIX. The line shows the theoretically calculated value.

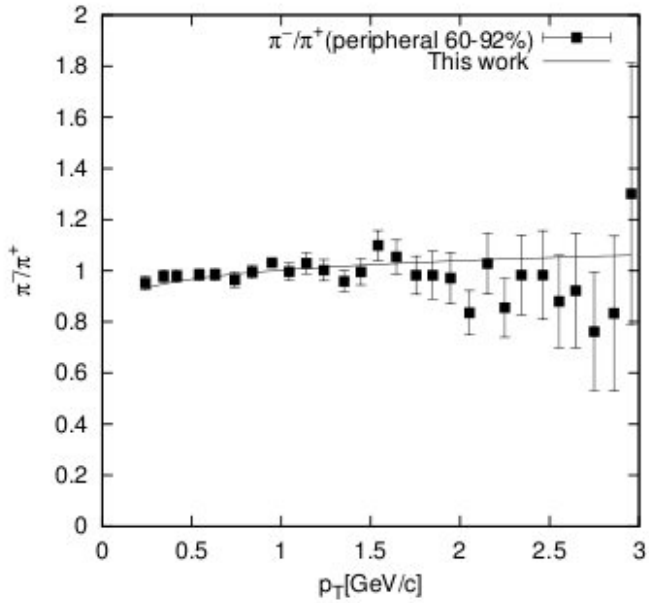

Fig. 26. The π^-/π^+ ratio behaviors at the peripheral reaction (60–92%). Data are taken from PHENIX. The line shows the theoretically calculated value.

3.5.2. *The K^-/K^+ ratios*

In a similar way, the expressions for K^-/K^+ for central (0–5%) and the peripheral reactions (60–92%) can be obtained from Figs. 7–10 and could be represented by

$$\left.\frac{K^-}{K^+}\right|_{\text{central}} = 0.947 p_T^{0.039} \tag{28}$$

and

$$\left.\frac{K^-}{K^+}\right|_{\text{peripheral}} = 0.940 p_T^{0.025}. \tag{29}$$

Figures 27 and 28 show the K^-/K^+ ratios in which the solid lines show the SCM-based calculated results against the experimental data taken from PHENIX.

3.5.3. *The $\bar{p}/p$ ratios*

Based on the SCM, the expressions for central and peripheral $\bar{p}/p$ ratios could be designated by

$$\left.\frac{\bar{p}}{p}\right|_{\text{central}} = 0.723 p_T^{0.044}, \tag{30}$$

$$\left.\frac{\bar{p}}{p}\right|_{\text{peripheral}} = 0.774 p_T^{-0.013}. \tag{31}$$

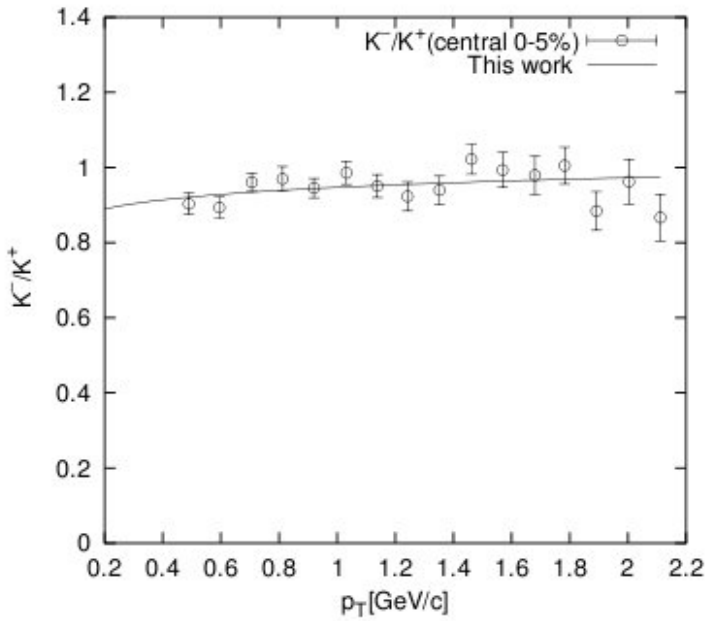

Fig. 27. The plot of central (0–5%) K^-/K^+ ratio behaviors. Data are taken from the PHENIX. Line shows the theoretical SCM based result.

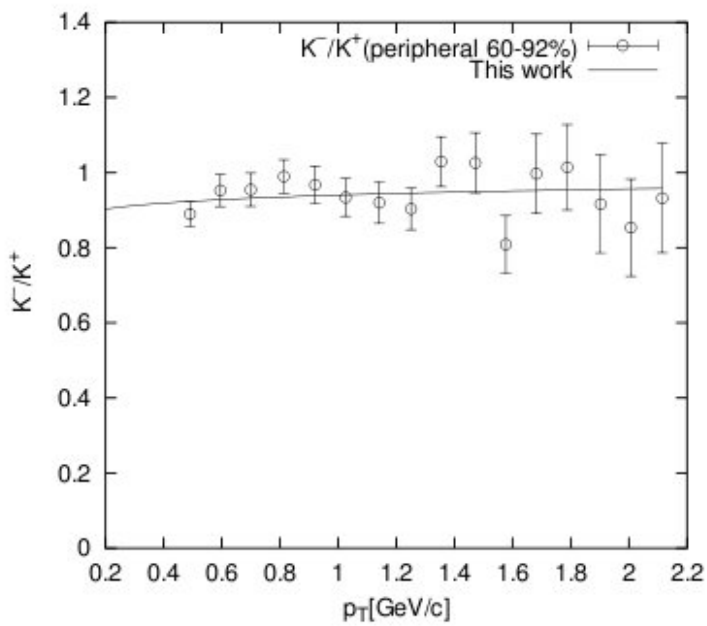

Fig. 28. The plot of peripheral (60–92%) K^-/K^+ ratio behaviors. Data are taken from the PHENIX. Line shows the theoretical SCM based result.

In Figs. 29 and 30 we have plotted $\bar{p}/p$ for central and peripheral reactions. The solid lines in those figures show the theoretical values while the dots show the experimental ones.

3.5.4. *The K/π ratios*

The expressions for K^-/π^- and K^+/π^+ in central and peripheral Au Au reaction are given by

$$\left.\frac{K^-}{\pi^-}\right|_{\text{central}} = 0.424 p_T^{1.304} \exp(-0.11 p_T^2)\,, \tag{32}$$

$$\left.\frac{K^-}{\pi^-}\right|_{\text{peripheral}} = 0.360 p_T^{1.022} \exp(-0.11 p_T^2)\,, \tag{33}$$

$$\left.\frac{K^+}{\pi^+}\right|_{\text{central}} = 0.452 p_T^{1.285} \exp(-0.11 p_T^2)\,, \tag{34}$$

$$\left.\frac{K^+}{\pi^+}\right|_{\text{peripheral}} = 0.379 p_T^{1.077} \exp(-0.11 p_T^2)\,. \tag{35}$$

We have plotted K^-/π^- and K^+/π^+ in Figs. 31 and 32, respectively. The theoretical curves are shown by the solid lines and the experimental points for central and the peripheral reactions are by filled and unfilled points respectively in those figures.

3.5.5. *The $\bar{p}/\pi$ and p/π ratios*

In a similar fashion, fits to the $\bar{p}/\pi$ and p/π ratios in the light of SCM are given hereunder:

$$\left.\frac{\bar{p}}{\pi}\right|_{\text{central}} = 0.195 p_T^{2.187} \exp(-0.11 p_T^2)\,, \tag{36}$$

$$\left.\frac{\bar{p}}{\pi}\right|_{\text{peripheral}} = 0.156 p_T^{1.462} \exp(-0.11 p_T^2)\,, \tag{37}$$

$$\left.\frac{p}{\pi}\right|_{\text{central}} = 0.259 p_T^{2.256} \exp(-0.11 p_T^2)\,, \tag{38}$$

$$\left.\frac{p}{\pi}\right|_{\text{peripheral}} = 0.223 p_T^{1.325} \exp(-0.11 p_T^2)\,. \tag{39}$$

Figures 33 and 34 show the $\bar{p}/\pi$ and p/π ratio behaviors in RHIC Au Au collisions. The solid lines are the theoretical fits against the experimental background.

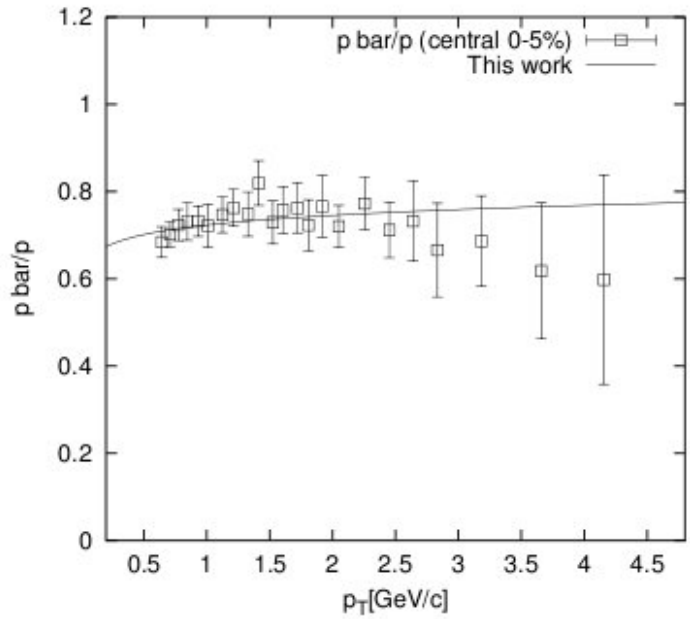

Fig. 29. The $\bar{p}/p$ ratio behaviors at the central reaction (0–5%). Data are taken from PHENIX. The line shows the theoretically calculated value.

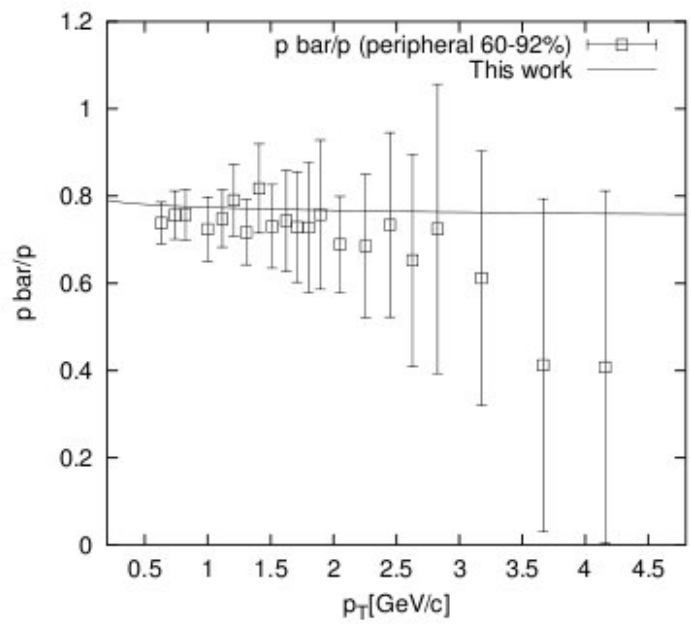

Fig. 30. The $\bar{p}/p$ ratio behaviors at the peripheral reaction (60–92%). Data are taken from PHENIX. The line shows the theoretically calculated value.

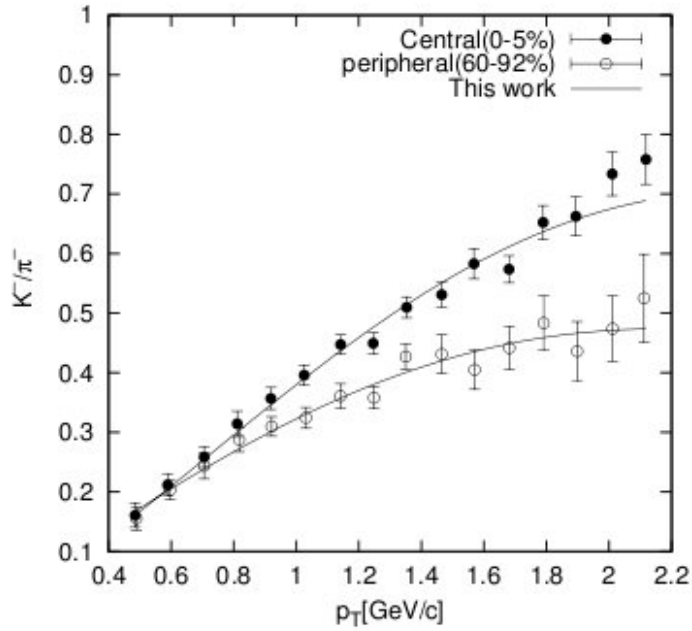

Fig. 31. Ratios of K^-/π^- as a function p_T for central (0–5%) and peripheral (60–92%) Au Au reactions at $\sqrt{s_{NN}} = 200$ GeV. The lines show the theoretical SCM results.

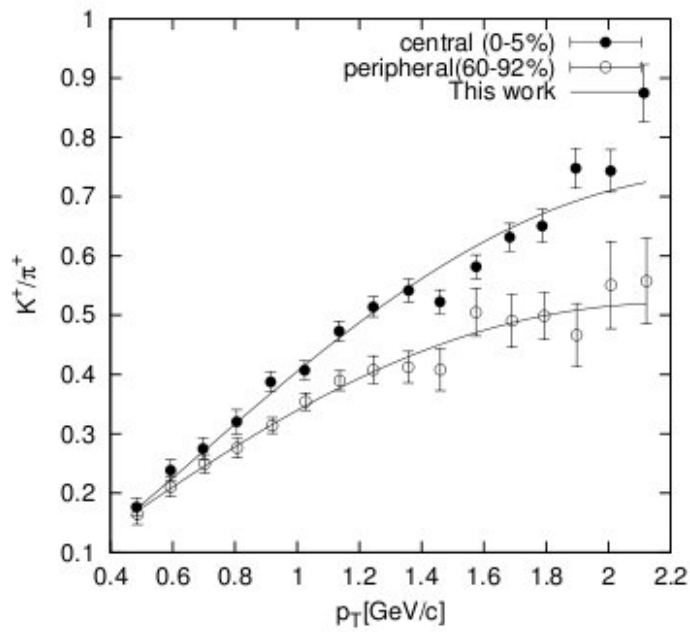

Fig. 32. Ratios of K^+/π^+ as a function p_T for central (0–5%) and peripheral (60–92%) Au Au reactions at $\sqrt{s_{NN}} = 200$ GeV. The lines show the theoretical SCM results.

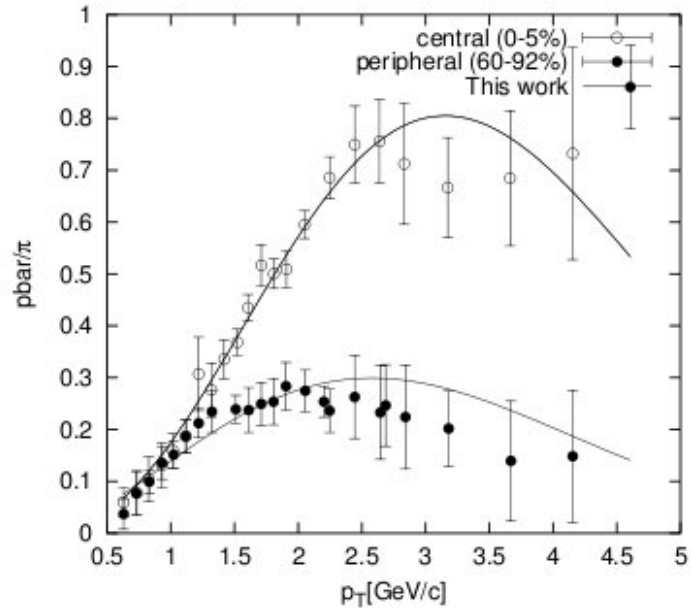

Fig. 33. $\bar{p}/\pi$ ratios as a function p_T for central (0–5%) and peripheral (60–92%) Au Au reactions at $\sqrt{s_{NN}} = 200$ GeV. The lines show the theoretical SCM results.

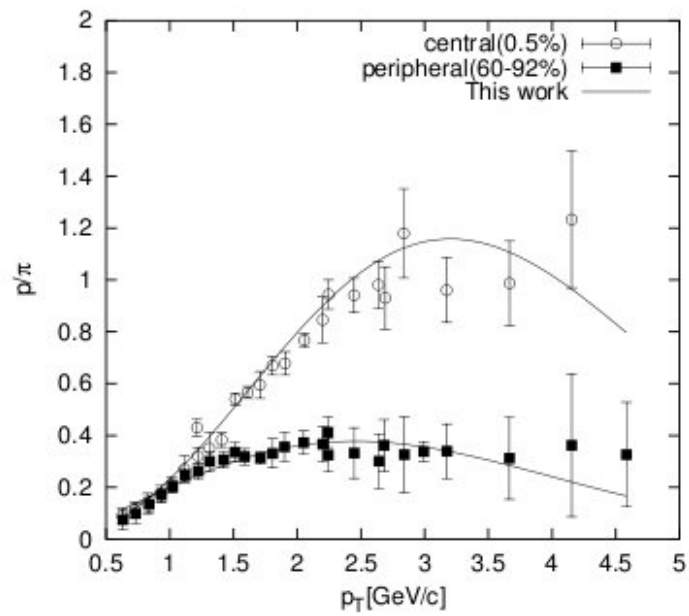

Fig. 34. p/π ratios as a function p_T for central (0–5%) and peripheral (60–92%) Au Au reactions at $\sqrt{s_{NN}} = 200$ GeV. The lines show the theoretical SCM results.

4. Discussions and Conclusions

The results imply the following few points of great physical importance: (i) even in nucleus–nucleus reactions at high energies and at large p_T, the proton–proton collisions constitute, according to our approach, the very basic interactions; (ii) as the nature cannot distinguish between "soft" and "hard" interactions, our working formulae, for even proton–proton collisions contain a mixed form with both exponential part indicating "soft" collisions and a power-law form of p_T-dependence depicting "hard"-ness of reactions; (iii) the results for nucleus-involved reactions could be obtained from the results based on pp-interactions by the Glauberian techniques which act as the connecting bridge between pp reactions and pA/AA reactions; (iv) the multiple gluonization cum radiation loss effects of the QCD-based standard model are taken care of here by the intensive partonic rearrangement term with multiple collision effects; (v) the model can explain behaviors of the p_T data without the so-called collective effects in the QCD-based and QGP-included approaches. (However, this statement is not to be viewed as the denial of the existence of the probable collective effects on the other observable(s). In fact, unless, the studies on the flow-behavior are taken up from the viewpoint of the SCM model, no categorical comment on the status of the collective effects would be justified.)

The basic model and some others as well used in the present work are surely of somewhat nonstandard variety. But the theoretical results obtained by the SCM, the flyover model and the Glauberian techniques are fairly in agreement with the measured data. The obtained ratio-values also agree well with measurements. And they provide the necessary crosschecks for the model-based results on p_T-spectra. Besides, the formulas arrived at here for pions, kaons and proton–antiprotons have exactly similar forms. The total approach, thus, might provide, in our opinion, an alternative route to understand and interpret the behavior of high energy collisions involving the NN, NA and AA interactions.

However, there are some limitations and shortcomings as well. The theoretical results on p_T-spectra for proton and antiproton production at relatively large-p_T values seem to be overdamped as the divergences between measured data and theoretical predictions at such transverse momentum values are considerably large. However, unless data for kaon–antikaons at such high transverse momentum values are obtained in the same or similar energy domain no clear pattern does emerge; and it is difficult to arrive at any firm conclusion on such deficiencies of the model. Besides, we fail to link up the "a" and "N_R" values in terms of any concrete relationship between these hand-inserted values and the impact parameter represented commonly by "b."

Despite these limitations and shortcomings, we have succeeded in giving a fair account of the impressive volume of experimental data in a comprehensive manner with even some clear consistency checkups. Apart from these important successes, we are driven to take up the studies on the SCM by the stimulating remarks of

Iwasaki *et al.*[41] "The existence of the QGP, which is predicted by QCD, has not been discovered in nature." Furthermore, in our opinion, the work assumes special significance *vis-a-vis* one conclusive comment made by Altarelli[42] on the status of the QGP. "However, for QGP, it is fair to say that the significance of each single piece of evidence can be questioned and one is still far from an experimental confirmation of the phase transition."

Acknowledgments

The authors express their thankful gratitude to the referee for his/her constructive suggestions in improving the earlier draft of the manuscript.

References

1. P. Steinberg, arXiv:0705.0382.
2. PHENIX Collab. (S. S. Adler *et al.*), *Phys. Rev. Lett.* **96**, 032301 (2006).
3. Star Collab. (H. J. Huang), *Int. J. Mod. Phys. A* **21**, 825 (2005).
4. Star Collab. (H. J. Huang), arXiv:nucl-ex/0608051.
5. M. J. Tanenbaum, *Rep. Prog. Phys.* **69**, 2005 (2006).
6. PHENIX Collab. (T. Chuzo *et al.*), *Eur. Phys. J. C* **49**, 23 (2007).
7. D. Porok, *Phys. Rev. C* **75**, 014903 (2007), arXiv:nucl-th/0609041.
8. PHENIX Collab. (S. S. Adler *et al.*), *Phys. Rev. C* **72**, 014903 (2005).
9. PHENIX Collab. (M. Shimomura *et al.*), *Nucl. Phys. A* **774**, 457 (2006).
10. PHENIX Collab. (S. S. Adler *et al.*), *Phys. Rev. Lett.* **94**, 232301 (2005).
11. PHENIX Collab. (S. S. Adler *et al.*), *Phys. Rev. Lett.* **97**, 052301 (2006).
12. R. C. Hwa, *Eur. Phys. J. C* **43**, 233 (2005).
13. T. Csorgo *et al.* (eds.), *Nucl. Phys. A* **774**, 1 (2006) [*Proc. 18th Int. Conf. Ultra-Relativistic Nucleus–Nucleus Collisions* (*QM2005*), Hungary, 4–9 August 2005].
14. R. Stock, *J. Phys. G: Nucl. Part. Phys.* **30**, S633 (2004).
15. D. Riche and G. Levin, *Nucl. Phys. A* **750**, 1 (2005).
16. J. I. Kapusta, arXiv:0705.1277.
17. U. Heinz and M. Jacob, nucl-th/0002042.
18. PHOBOS Collab. (G. Ronald *et al.*), *Nucl. Phys. A* **774**, 113 (2006).
19. BRAHMS Collab. (I. Arsen *et al.*), *Nucl. Phys. A* **757**, 1 (2005).
20. STAR Collab. (J. Adams *et al.*), *Nucl. Phys. A* **757**, 102 (2005).
21. PHOBOS Collab. (B. B. Back *et al.*), *Nucl. Phys. A* **757**, 28 (2005).
22. H. Nastase, arXiv:hep-th/0501068.
23. P. Bandyopadhyay and S. Bhattacharyya, *Il Nuovo Cimento A* **43**, 305 (1978).
24. P. Bandyopadhyay, R. K. Roychoudhury, S. Bhattacharyya and D. P. Bhattacharyya, *Il Nuovo Cimento A* **50**, 133 (1979).
25. S. Bhattacharyya and P. Pal, *Il Nuovo Cimento C* **9**, 961 (1986).
26. S. Bhattacharyya, *Il Nuovo Cimento C* **11**, 51 (1988).
27. S. Bhattacharyya, *J. Phys. G* **14**, 9 (1988).
28. S. Bhattacharyya, *Hadronic J.* **11**, 85 (1988).
29. M. Imachi *et al.*, *Suppl. Prog. Theor. Phys.* **48**, 101 (1971).
30. P. Guptaroy, B. De, S. Bhattacharyya and D. P. Bhattacharyya, *Fizika B* **11**, 115 (2002).
31. P. Guptaroy, B. De, S. Bhattacharyya and D. P. Bhattacharyya, *Int. J. Mod. Phys. E* **12**, 493 (2003).

32. P. Guptaroy, B. De and S. Bhattacharyya, *Int. J. Mod. Phys. A* **18**, 5047 (2003).
33. P. Guptaroy, B. De and S. Bhattacharyya, *Heavy Ion Phys.* **17**, 167 (2003).
34. P. Guptaroy, B. De, G. Sanyal and S. Bhattacharyya, *Int. J. Mod. Phys. A* **20**, 5037 (2005).
35. C. Y. Wong, *Introduction to High-Energy Heavy Ion Collisions* (World Scientific, 1994).
36. K. Kadija, I. Derado, N. Schmitz and P. Seyboth, *Z. Phys. C* **66**, 373 (1995).
37. A. Bialas, M. Bleszynki and W. Czyz, *Nucl. Phys. B* **111**, 461 (1976).
38. NA50 Collab. (M. C. Abreu *et al.*), preprint, CERN-EP/2002-017 (2002).
39. PHENIX Collab. (S. S. Adler *et al.*), *Phys. Rev. C* **69**, 034909 (2004) [also at arXiv:nucl-ex/0307022].
40. Particle Data Group, *Eur. Phys. J. C* **15**, 211 (2000).
41. M. Iwasaki, H. Ohnishi and T. Fukutom, hep-ph/0703271.
42. G. Altarelli, to appear in *Proceedings of IFAE 2006*, Pavia, Italy, arXiv:hep-ph/0609097.